Published by :
https://www.ijert.org/
An International Peer-Reviewed Journal

International Journal of Engineering Research & Technology (IJERT)
ISSN: 2278-0181
Vol. 15 Issue 03 , March - 2026

Fatigue Life Assessment of 90° Miter Bends under Resonant Vibration Using Strain Gauge Measurements and Numerical Analysis

Nirav Rathod
Research Scholar, Gujarat Technological University,
Ahmedabad- 382424, Gujarat, India

Dr. Dilip Patel
GIDC Degre Engineering College, Mechanical Engineering Department, Navsari-396406, Gujarat, India

***Abstract*—Miter bends exhibit significant stress concentrations at geometric discontinuities, making them prone to fatigue failure under resonant conditions. This study presents a strain-based fatigue life assessment integrating Finite Element Analysis (FEA) and experimental validation. Modal analysis was performed by conducting numerical investigation to obtain natural frequencies and mode shapes, which were used as inputs for harmonic response analysis to identify critical locations. Experimental testing was conducted on a fixed–free setup under combined dead weight and resonant excitation using strain gauges and a load cell. Crack initiation was detected through strain spikes and confirmed using Magnetic Particle Testing (MPT). Measured microstrain was converted into stress, and fatigue life was evaluated using these experimental stress amplitudes. A Basquin S–N relation, calibrated all miter specimens, shows strong agreement with harmonic-FEA life. The model demonstrated excellent predictive accuracy, explaining 99.5% of the variance in $log_{10}N$ ($R^2 = 0.995$). The RMSE was approximately 0.021, while the Mean Absolute Percentage Error (MAPE) and Median Absolute Percentage Error (MdAPE) were 3.7% and 2.9%, respectively, indicating high precision and robustness. A close agreement was observed among fatigue life results obtained from experimental measurements, Basquin-based analytical estimation, and numerical (FEA) analysis.**

Keywords*— *Miter bend fatigue, Resonant vibration, Hot-spot stress, Strain based fatigue analysis

I. INTRODUCTION

Mitered pipe bends fabricated by joining straight segments at prescribed cut angles remain a cost-effective alternative to smooth elbows in space-constrained piping layouts across process, power, and materials-handling industries. The geometric discontinuities introduced by the cut planes and weld toes intensify local stresses, especially at the intrados and crotch regions, which makes fatigue under cyclic loading a credible limiting mechanism for service life. In vibration-prone environments, even modest background forcing can align with a structural mode of the piping run, amplifying local strain and accelerating crack initiation at these hot-spots. Consequently, design-relevant life assessment must resolve local stress/strain metrics at the controlling locations rather than rely solely on global load surrogates.

While analytical intensification factors and global S–N rules of thumb can provide screening insight, their predictive skill degrades when resonant vibration and fixture-specific boundary conditions (e.g., fixed–free spans, deadweight bias, attachments) dominate response. In such cases, physics-informed assessment benefits from (i) finite element (FE) modal analysis to identify mode shapes and natural frequencies, (ii) harmonic analysis to quantify hot-spot stress amplitudes at resonance, and (iii) direct experimental validation using strain gauges placed at FE-identified hot-spots. This integration enables one-to-one comparison at the gauge footprint, reduces model-form ambiguity, and creates calibration-grade data for life modeling and uncertainty quantification.

Table 1: Factor Information

Factors	Levels	Values
Number of Welds	3	1W, 2W, 3W
Pipe Outside Diameter (OD)	3	141.3 mm, 219.1 mm, 323.8 mm
Pipe Thickness (t)	3	0.511 mm, 0.9 mm, 1.2 mm

Table 2: Structural parameters of Miter bends

3W (Three Weld)			2W (Two Weld)			1W (One Weld)		
Specimen Number	OD (mm)	t (mm)	Specimen Number	OD (mm)	t (mm)	Specimen Number	OD (mm)	t (mm)
1	323.8	0.511	10	323.8	0.511	19	323.8	0.511
2	323.8	0.9	11	323.8	0.9	20	323.8	0.9

International Journal of Engineering Research & Technology (IJERT)
ISSN: 2278-0181
Vol. 15 Issue 03 , March - 2026

3	323.8	1.2	12	323.8	1.2	21	323.8	1.2
4	219.1	0.511	13	219.1	0.511	22	219.1	0.511
5	219.1	0.9	14	219.1	0.9	23	219.1	0.9
6	219.1	1.2	15	219.1	1.2	24	219.1	1.2
7	141.3	0.511	16	141.3	0.511	25	141.3	0.511
8	141.3	0.9	17	141.3	0.9	26	141.3	0.9
9	141.3	1.2	18	141.3	1.2	27	141.3	1.2

The present study advances this integrated approach for 90° miter bends by executing a combined experimental and numerical program on 27 specimens across practical diameter-thickness combinations and weld configurations as shown in Table 1 and Table 2. First, a parametric FE model—meshed with local refinement at weld toes and crotch—was subjected to modal and harmonic analyses to locate and prioritize instrumentation sites. Second, each specimen was tested on a fixed–free rig in which deadweight provided a mean bending bias and electromagnetic excitation drove the structure at its measured resonant frequency. Third, three strain gauges were bonded at the FE-identified hot-spots, and the applied load was monitored using an S-type load cell; all channels were recorded on a four-channel data logger at 1-s sampling for the full duration of each test. Crack initiation was operationally defined as the moment of a distinct strain spike in the hot-spot time history and was verified by magnetic particle testing (MPT), ensuring a consistent, defensible definition of NNN (cycles to initiation, not final fracture) across the matrix.

The life modeling adopts a stress–life (S–N) framework appropriate for the predominantly high-cycle, resonance-dominated regime of interest. Specifically, Basquin relation in log–log space is best suitable for complex miter bend configurations as shown in Equation 1, which captures the nonlinear sensitivity of life to hot-spot stress amplitude and aligns with observed metallic fatigue phenomenology.

$$log_{10}N = A + B\ log_{10}\sigma \tag{1}$$

where N represents the number of cycles to failure, σ is the experimentally obtained stress amplitude, and A and B are material constants. The model is complemented with 95% prediction bands to support design checks and risk-informed decisions (e.g., whether predicted hot-spot stress falls within an acceptable life envelope).

A central goal of the research paper is to quantify and reduce model uncertainty by validating FE hot-spot predictions against co-located gauge measurements. Von Mises stresses have been extracted at the gauge footprints and evaluate parity using metrics appropriate for fatigue data R Square (R^2) in $log_{10}N$, RMSE in $log_{10}N$, and absolute percentage errors and by inspecting residual distributions for bias and heteroscedasticity. This parity-first discipline reveals whether residual scatter stems from measurement (gauge, wiring, sampling), geometry (weld-toe radius, local surface condition, residual stress), or model form (mesh density near the toe, harmonic linearization). The result is a calibrated, mechanics-first life model that avoids the pitfalls of naive regression on geometric descriptors alone.

II. LITERATURE REVIEW

Compared with smooth elbows, mitered bends exhibit discontinuity stresses at cut planes together with cross-section ovalization under bending/pressure, which elevates local flexibility and hot-spot stress. A comprehensive review of mitred-bend behavior highlights gaps for combined loading, end effects, and vibration-induced fatigue, motivating targeted experimental and FE work [1,2]. For smooth elbows, an overview of bend mechanics emphasizes in-plane/out-of-plane bending, pressure–bending interaction, and fatigue at flank hot-spots—mechanisms that also underpin miter response [3]. Nonlinear FE investigations focused on mitered elbows quantify elastic–plastic capacity, failure modes, and the effect of internal pressure, informing design envelopes in geohazard and seismic contexts [4].

Within process piping, ASME B31.3 governs pressure design of miters, while vibration acceptance relies on engineering assessment; practical notes and discussions document sensitivity of allowable pressure to segment geometry and the usefulness of FE verification. Summaries of layout/fabrication constraints (number of cuts, bend radius, service limits) consolidate B31.3 applications for mitered components [5,15].

Under strong cyclic loading, elbows—and by analogy, mitered bends—show localized plasticity, pronounced ovalization, and crack initiation at intrados/crotch hot-spots. Controlled in-plane cyclic tests established strain-based low-cycle fatigue curves and benchmarked nonlinear FE models with advanced plasticity, offering an experimental–numerical template for resonance-dominated conditions [7]. For mitered bends, combined in-plane bending with internal pressure has been used to study ratcheting and fatigue; results underline sensitivities to cyclic hardening laws and the need to explicitly treat crack initiation/propagation in simulations

International Journal of Engineering Research & Technology (IJERT)
ISSN: 2278-0181
Vol. 15 Issue 03 , March - 2026

[5]. Complementary limit-load and shakedown maps for 90° miters provide bounding domains for cyclic response under combined actions [6].

In the high-cycle domain, Basquin's law provides a power-law S–N relation fitted in log–log space and remains the canonical basis for stress-life calibration [8]. For low/medium cycles with plasticity, strain-life formulations (Coffin–Manson and Morrow) relate elastic and plastic strain amplitudes to life and are widely adopted in design practice and teaching resources [9]. When non-zero mean stress is present (e.g., deadweight or pressure bias), the SWT parameter is commonly used to correct initiation life; recent reviews discuss variants and applicability across metals and loading states [10]. For notched/welded details typical of miter weld toes, local elastoplastic estimation methods (e.g., Neuber-type rules) help translate nominal response to hot-spot strain/stress for life evaluation [11].

ASME B31.3 requires designs to avoid vibration-induced fatigue but does not prescribe a single acceptance criterion; current practice therefore adopts the Energy Institute (EI) AVIFF guidelines and industry experience to assess severity, plan walkdowns, and implement mitigations (detuning, bracing, redesign) [12], [13]. Case histories and training material emphasize that vibration remains a frequent root cause of piping failures and advocate a structured, stepwise approach—directly relevant to resonance-dominated miter bends [13].

III. EXPERIMENTAL INVESTIGATION

A. Specimens and Geometry

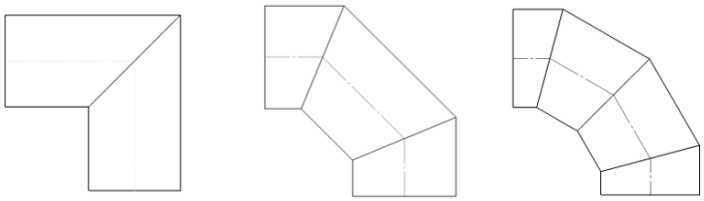

Fig. 1. 1 Weld (1W), 2 Weld(2W), 3 Weld (3W) Miter Bends

The research paper involves the fabrication of 90° miter bend specimens to investigate the effect of geometric parameters on fatigue behavior. Fig. 1 illustrates the configurations of specimens with different numbers of welds, namely 1W, 2W, and 3W. Miter bends were manufactured by cutting straight pipe sections at predefined angles and joining them through welding to achieve a 90° bend configuration. Key parameters such as pipe outer diameter (OD), wall thickness, and number of weld joints were systematically varied to examine their influence on structural performance. Multiple specimens were prepared with different combinations of these parameters to ensure a comprehensive experimental dataset. The variation in thickness and diameter alters the stiffness and stress distribution, while the number of welds introduces additional discontinuities, potentially affecting fatigue life. This controlled fabrication approach enables a detailed assessment of how geometric and weld-related factors contribute to the overall mechanical response of miter bends under loading conditions. Miter-bend specimens covering outside diameter, number of welds and thickness ranges were fabricated as per ASME B36.10M; weld quality and dimensions were verified by Coordinate Measuring Machine and NDT before testing as shown in Fig. 2.

Fig. 2. Verification of Dimensions using coordinate measuring machine (CMM)

B. Instrumentation and Data Acquisition

Sensors and channels

International Journal of Engineering Research & Technology (IJERT)
ISSN: 2278-0181
Vol. 15 Issue 03 , March - 2026

- Strain gauges: Strain gauges were bonded at the finite element (FE) identified hot spots, namely the intrados, crotch, and crown (extrados) in accordance with hot spot stress practice, ensuring that the gauge locations coincide with the FE extraction points. This enables a direct one-to-one comparison between experimental and FE stresses at the weld toe/edge.
- Load channel: S-type load cell suspended at the free end to apply/monitor deadweight.
- Data Acquisition System: 4-channel data logger, sampling at 1 s (three strain + one load). The voltage range 0–10 V, 24-bit counts (Max Count = 16,777,216), excitation 5–10 V, gauge factor (GF) and conversion factor used for strain conversion. A four channel data logger was used with a sampling interval of 1 second, in which three channels recorded strain and one channel recorded load. The system operated within a voltage range of 0 to 10 V with 24 bit resolution corresponding to a maximum count of 16,777,216. An excitation voltage in the range of 5 to 10 V was supplied to the strain gauges, and the measured signals were converted into strain using the gauge factor and an appropriate conversion factor.
- Vibrometer is installed to measure the real-time excitation frequency for each specimen.

Electromagnetic exciter and adjustable fixture

- The miter bend is tested in fixed–free configuration. At the free end, steel plates are attached below the bend; beneath these plates a stationary electromagnetic vibrating coil is mounted on an adjustable-height fixture. The vertical adjustment accommodates different bend radii and maintains a constant air gap between plate and coil across specimens.
- The vibration controller drives the exciter; frequency is swept to the measured natural frequency (from modal check) and then held (or stepped) under constant amplitude to promote resonant response. Amplitude set-points are chosen to reach target hot-spot strain without violating rig limits. *(Real-time verification via the vibrometer ensures the command frequency equals the physical response.)*

Calibration

- Strain measurements were derived from raw sensor data using applied gauge factors (GF) and conversion coefficients. Instrument reliability was ensured through apparatus-based gauge calibration and the data logger's internal calibration protocol.
- S-type load cell: multi-point calibration against certified masses over the operating range; zero balance checked before each run.

C. Strain-Stress Conversion and Life Extraction

The data acquisition system records the strain gauge output in the form of digital counts, which are proportional to the analog signal after analog-to-digital conversion. These counts are first converted into a corresponding change in voltage (ΔV) using the calibration factor or resolution of the data logger. The obtained voltage change is then related to mechanical strain using the gauge factor (GF) of the strain gauge, which defines the sensitivity of the gauge to deformation. Alternatively, a calibration or conversion constant (K) may be used, which accounts for the complete measurement system, including bridge configuration and excitation voltage. This sequential conversion from counts to voltage and then to strain enables accurate determination of the strain induced in the specimen.

D. Methodology

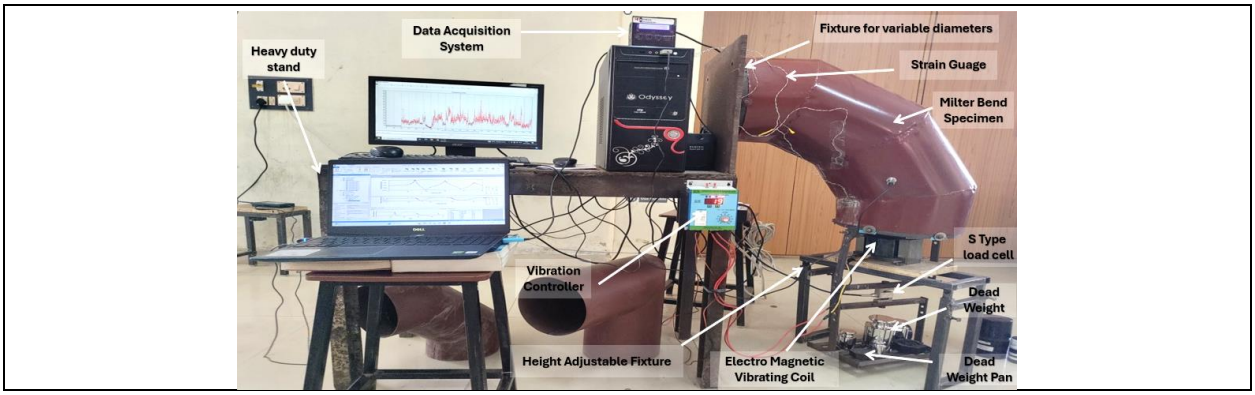

International Journal of Engineering Research & Technology (IJERT)
ISSN: 2278-0181
Vol. 15 Issue 03 , March - 2026

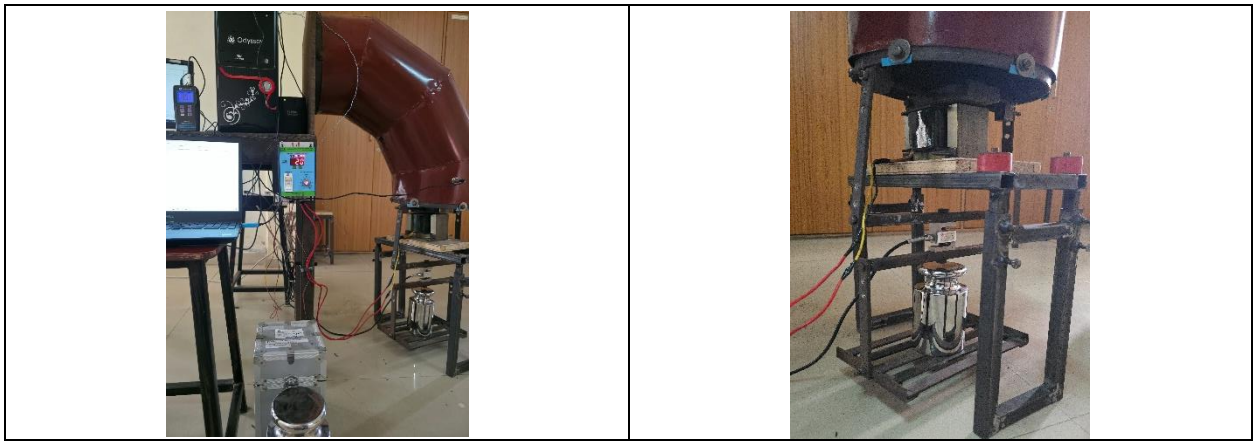

Fig. 3. Experimental Test Rig

The experimental test rig setup used for fatigue testing is illustrated in Fig. 3. Vibration was induced in the Y-direction using an electromagnetic vibrating coil, tuned to the specimen's resonant frequency determined via modal analysis. Strain gauges were placed at critical locations (weld toes, crown, intrados, extrados) based on FEA stress maps. A 4-channel data logger recorded strain and load data at 1-second intervals, enabling real-time monitoring of fatigue progression. Crack initiation was confirmed through visual inspection and NDT.

A four-channel data logger was employed to record strain gauge and load measurements at a sampling interval of one second. Three channels were assigned to strain gauges, which measured voltage variations later converted to microstrain using the strain gauge factor and conversion factor. The strain gauges were positioned at three critical locations on the miter bend, as identified through finite element analysis (FEA), to monitor strain behavior under loading. Among these locations, one or two points exhibited higher strain magnitudes, indicating regions more prone to crack initiation. To validate these observations, non-destructive testing (NDT) was carried out on the specimens. The fourth channel of the data logger was connected to an S-type load cell to capture real-time loading data.

The data logger output exhibits a distinct peak at the point of crack initiation, indicating the moment when a crack is most likely to appear in the specimen as shown in Fig.4 for one of the test specimen. The corresponding time recorded at this peak is considered the fatigue life of the component under the applied loading conditions.

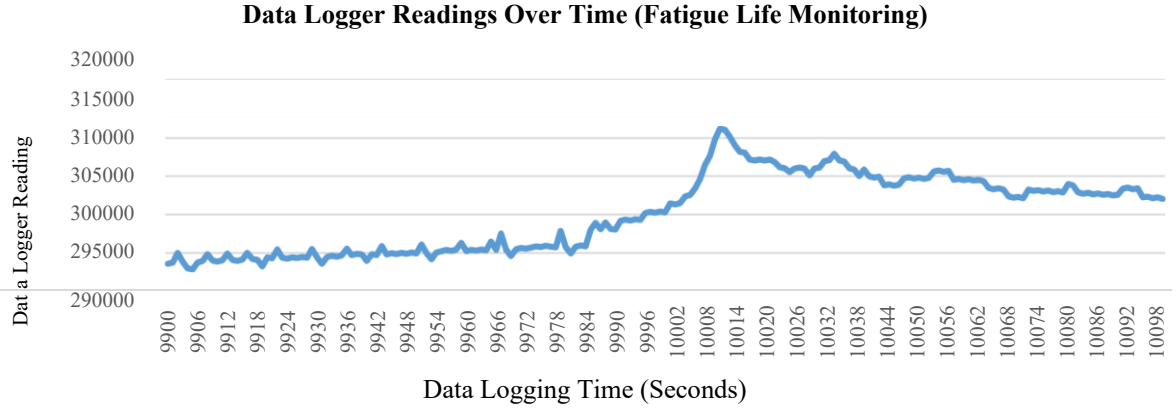

Fig. 3. Fatigue Life Monitoring

Table 3 depicts the fatigue life of miter bends subjected to combination of dead load and resonant frequency.

Table 3: Experiment Readings

Specimen 1-9			Specimen 10-18			Specimen 19-27		
Measured Strain (µε)	Stress (MPa)	Fatigue Life (Cycles)	Measured Strain (µε)	Stress (MPa)	Fatigue Life (Cycles)	Measured Strain (µε)	Stress (MPa)	Fatigue Life (Cycles)
750.79	157.67	1.37E+06	706.88	148.45	1.18E+06	758.03	159.19	8.46E+05

International Journal of Engineering Research & Technology (IJERT)
ISSN: 2278-0181
Vol. 15 Issue 03 , March - 2026

541.62	113.74	1.80E+06	484.69	101.78	1.40E+06	470.48	98.80	1.16E+06
564.06	118.45	5.33E+06	419.96	88.19	3.01E+06	273.30	57.39	9.67E+05
1293.21	271.57	2.01E+06	1160.64	243.73	8.54E+05	1049.23	220.34	4.32E+05
685.22	143.90	3.55E+06	709.32	148.96	2.01E+06	676.07	141.98	9.68E+05
631.25	132.56	4.43E+06	564.54	118.55	3.13E+06	564.76	118.60	1.97E+06
1362.86	286.20	1.20E+06	1466.60	307.99	8.19E+05	1671.91	351.10	5.02E+05
890.24	186.95	2.07E+06	1047.27	219.93	1.20E+06	1264.72	265.59	5.69E+05
685.39	143.93	4.90E+06	798.75	167.74	2.70E+06	996.39	209.24	9.51E+05

Magnetic particle testing (MT) was subsequently performed, and the detected surface cracks correlated well with the critical zones identified from the strain and FEA data as shown in Fig.5. Representative images from the magnetic particle inspection are shown below.

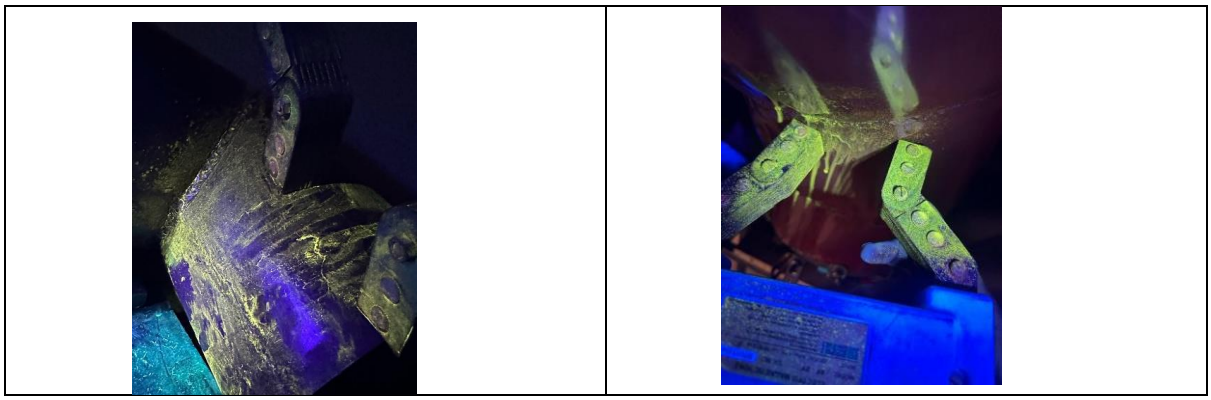

Fig.5. Magnetic Particle Test

IV. FINITE ELEMENT ANALYSIS

In this study, the miter bend was modeled with one end fixed and the other end free as shown Fig. 6. The free end was subjected to a combination of resonant vibrations and a deadweight (tensile loading), replicating realistic industrial conditions. These conditions simulate situations where miter bends experience vibrations due to inadequate support, variations in fluid density and viscosity, and other structural irregularities. The deadweight loading represents the effect of additional static loads, such as those imposed by attached valve assemblies or other components. Hence, a fixed–free boundary condition was adopted for the numerical investigation to estimate the fatigue life of the miter bend as shown in figure.

FEA was performed using ANSYS Workbench to simulate the dynamic response of each specimen [13]. A hexahedral mesh was utilized for the numerical investigation of miter bends to achieve higher accuracy in capturing their complex structural behavior. Miter bends are characterized by sharp geometric transitions and stress concentration zones, particularly along the weld lines and junctions of the bend segments. The use of hexahedral elements ensures better resolution of these localized stresses compared to tetrahedral meshing, which can introduce numerical inaccuracies in such regions. The structured nature of hexahedral meshing enhances element quality, minimizes distortion, and provides improved convergence during both static and dynamic simulations. Moreover, hexahedral meshes offer an optimal balance between computational efficiency and accuracy, making them well-suited for evaluating the fatigue life of miter bends subjected to combined resonant vibration and deadweight loading [14].

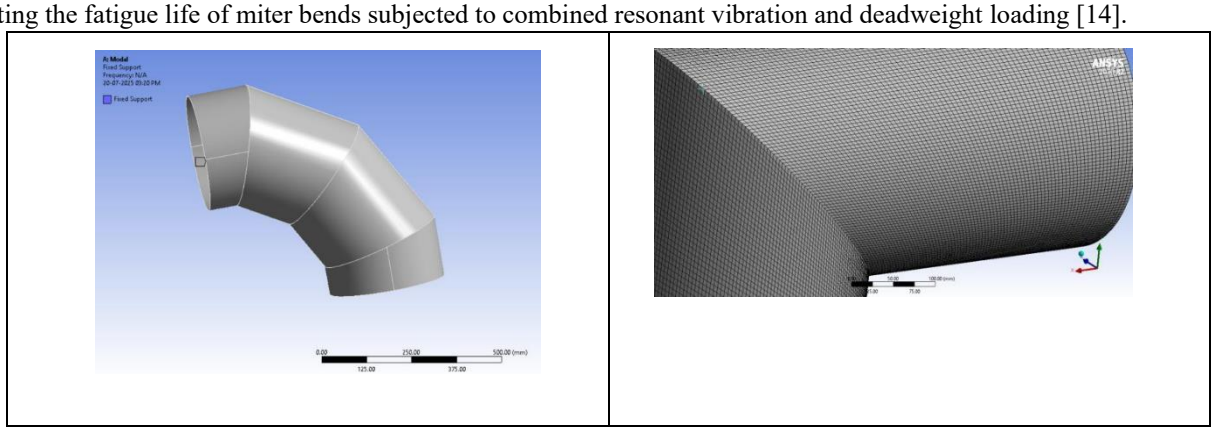

Fig. 6. Boundary Conditions and Discretization

International Journal of Engineering Research & Technology (IJERT)
ISSN: 2278-0181
Vol. 15 Issue 03 , March - 2026

A. Modal Analysis

Modal analysis was first performed to determine the natural frequencies and corresponding mode shapes of each specimen, as summarized in Table 1. Identifying these frequencies is essential because they represent the resonant conditions under which dynamic amplification of stresses can occur. These natural frequencies were subsequently used as excitation inputs in harmonic analysis to simulate the specimen's response under steady-state sinusoidal loading. The harmonic analysis provided detailed insights into the frequency-dependent behaviour, including displacement amplitudes, strain and stress distributions at critical regions, and potential stress concentration zones. Furthermore, these results served as the basis for fatigue life estimation under resonant conditions, enabling a comprehensive understanding of the structural integrity and durability of the miter bends when subjected to combined loading scenarios [15].

B. Harmonic Analysis

The harmonic response analysis was performed using the modal analysis results as inputs. The natural frequencies and corresponding mode shapes obtained from the FEA-based modal analysis were used to define the excitation range and boundary conditions [16,17]. This enabled accurate evaluation of stress amplitudes under dynamic loading for fatigue life prediction. Table 4 depicts the results of harmonic investigation of all miter bend specimens.

Table 4: Harmonic Analysis

Specimen Number	Vibrating Frequency (Hz)	Von Mises Stress (MPa)	Fatigue Life (10^6 Cycles)	Specimen Number	Vibrating Frequency (Hz)	Von Mises Stress (MPa)	Fatigue Life (10^6 Cycles)	Specimen Number	Vibrating Frequency (Hz)	Von Mises Stress (MPa)	Fatigue Life (10^6 Cycles)
1	137.01	165.36	1.41	10	120.87	155.815	1.11	19	106.78	146.27	0.862
2	181.98	118.15	1.82	11	156	113.13	1.49	20	128.52	108.11	1.16
3	176.84	121.17	5.67	12	151	91.8635	3.03	21	120.49	62.557	0.978
4	246.39	278.97	2.03	13	149.2	250.27	0.879	22	134.46	221.57	0.477
5	245.85	153.16	3.35	14	186.1	150.935	1.98	23	128.53	148.71	0.977
6	235.62	140.24	4.44	15	185.2	131.87	3.13	24	138.58	123.5	2.07
7	400.68	295.91	1.38	16	316.2	318.495	0.892	25	235.19	341.08	0.520
8	360.03	191.82	2.15	17	295	231.94	1.26	26	229.64	272.06	0.584
9	357.24	152.2	4.99	18	302.52	183.59	2.71	27	249.48	214.98	0.982

The finite element analysis (FEA) results for Specimen number 27 are presented in Fig. 7. The finite element analysis (FEA) results identified the most highly stressed region of the miter bend, which served as the location for strain gauge placement during the experimental study. This region was subsequently monitored to evaluate strain response and fatigue life under the specified combined loading conditions.

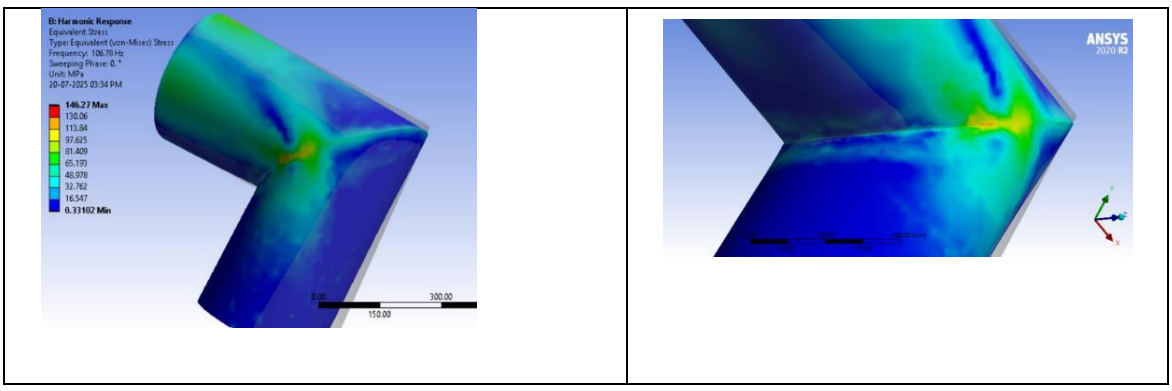

Fig. 7. Harmonic Response (Specimen 19)

International Journal of Engineering Research & Technology (IJERT)
ISSN: 2278-0181
Vol. 15 Issue 03 , March - 2026

The close agreement between the experimental and FEA results as depicted in Fig. 8 validates the reliability of the simulation approach in predicting fatigue life, with minor discrepancies explainable by physical and material variabilities inherent in real specimens.

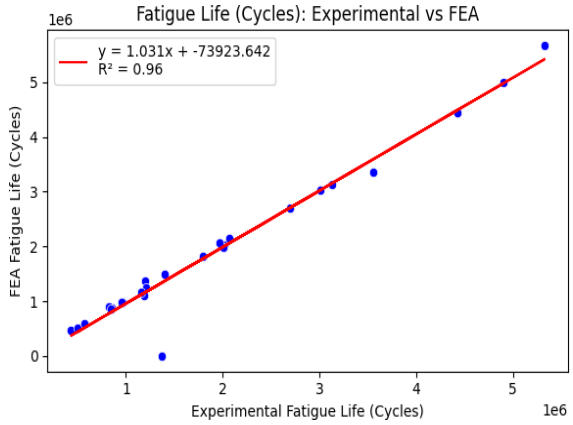

Fig.8. Fatigue Life (Cycles)

The fatigue life predicted through numerical analysis was further validated using experimental measurements obtained from strain gauges. The recorded microstrain values were converted into corresponding stress amplitudes using Hooke's law, considering the material's elastic properties. These experimentally derived stress values were then compared with the stress amplitudes obtained from the harmonic response analysis and those used in the calibrated Basquin S–N relation.

Fatigue life estimation, however, was also carried out using Basquin S-N relation [18]. The microstrain values recorded from strain gauges were converted into stress amplitudes using Hooke's law. These experimentally derived stress amplitudes were then used in the Basquin S–N relationship to evaluate fatigue life.

This approach ensures that the fatigue life prediction is grounded in actual measured response, while the FEA results are primarily used to understand the dynamic behavior of the structure. Table 4 presents a comparison of fatigue life obtained experimentally, analytically using the Basquin S–N relation, and numerically through FEA. The reported fatigue life results are scaled and expressed as the number of cycles in multiples of 10^6 for clarity and ease of comparison. The results show good agreement among all three methods, thereby validating the adopted approach for fatigue life estimation. A Basquin-type relation was fitted to the experimental data to provide a simplified design equation, and the corresponding 95% prediction bands are also reported.

$$log_{10}N = 7.771 - 0.721log_{10}\sigma \quad (2)$$

$$N = 5.90 \times 10^7 \, \sigma^{-0.72} (\sigma \text{ in MPa}) \quad (3)$$

Table 4: Fatigue Life Comparisons

Specimen Number	Experimental Fatigue Life	Basquin Fatigue Life	FEA Fatigue Life	Specimen Number	Experimental Fatigue Life	Basquin Fatigue Life	FEA Fatigue Life	Specimen Number	Experimental Fatigue Life	Basquin Fatigue Life	FEA Fatigue Life
1	1.37	1.49	1.41	10	1.18	2.72	1.11	19	0.85	1.35	0.862
2	1.80	38.98	1.82	11	1.40	118.35	1.49	20	1.16	159	1.16
3	5.33	25.97	5.67	12	3.01	496.27	3.03	21	0.97	36427	0.978
4	2.01	0.01	2.03	13	0.85	0.02	0.879	22	0.43	0.05	0.477
5	3.55	3.71	3.35	14	2.01	2.63	1.98	23	0.97	4.24	0.977
6	4.43	8.43	4.44	15	3.13	25.75	3.13	24	1.97	25.6	2.07
7	1.20	2.70	1.38	16	0.82	1.60	0.892	25	0.50	2.80	0.520
8	2.07	0.27	2.15	17	1.20	0.05	1.26	26	0.57	0.01	0.584
9	4.90	3.70	4.99	18	2.70	0.80	2.71	27	0.95	0.09	0.982

International Journal of Engineering Research & Technology (IJERT)
ISSN: 2278-0181
Vol. 15 Issue 03 , March - 2026

Fatigue life predicted using the Basquin equation was higher than experimental and FEA results for some specimens due to its assumption of ideal, uniform stress conditions as shown in Fig. 9. It does not account for stress concentrations, weld effects, and material imperfections, leading to overestimation compared to more realistic experimental and numerical approaches.

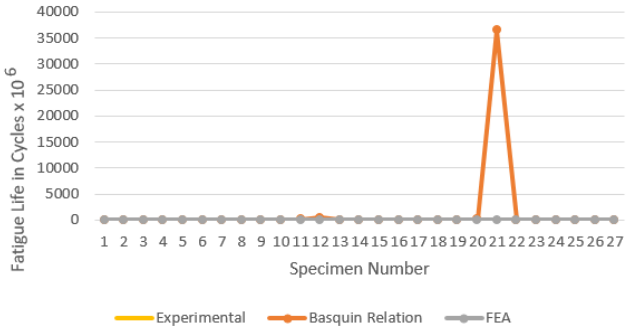

Fig. 9. Fatigue Life Comparison

A close agreement among the experimental stress, FEA-predicted stress, and Basquin-based stress confirmed the reliability of the numerical model and the adopted fatigue life estimation approach. This validation establishes consistency between experimental observations and analytical predictions, thereby strengthening the accuracy of the fatigue life assessment of the fabricated 90° miter bend specimens. The predicted peak frequency and response level were compared with the vibrometer-measured resonance and strain-gauge amplitudes; the resulting hot-spot stresses and fatigue lives were then benchmarked against the experimental life.

V. RESULTS

A. S–N Calibration with 95% Prediction Band

The experimental S–N fit and 95% prediction band shown in Fig. 10. The band supports design checks, if predicted hot-spot stress sits above the band, mitigation is required.

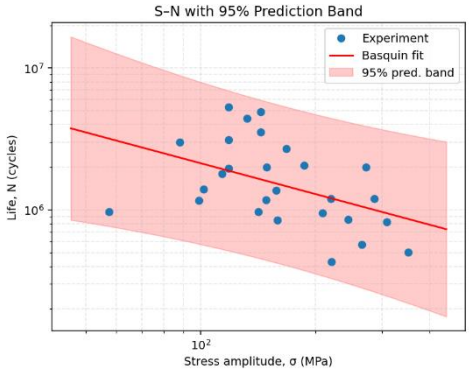

Figure 10: S-N Prediction Bend

B. Parity with Factor-of-Two Bands (FEA vs Experiment)

Life parity (log–log) with ±×2 guide bands demonstrates tight agreement in log space as shown in Fig.11.

International Journal of Engineering Research & Technology (IJERT)
ISSN: 2278-0181
Vol. 15 Issue 03 , March - 2026

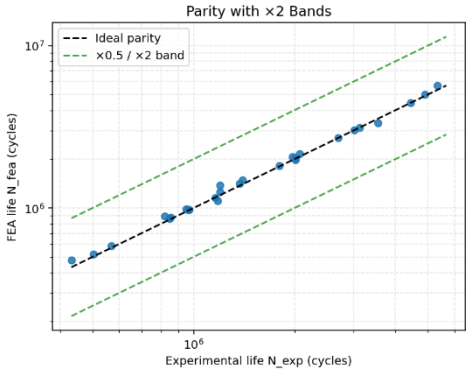

Fig. 11. Parity Plot with Factor-of-Two Bands for Fatigue Life (FEA vs Experimental)

Overall statistics: $R^2(\log_{10}N) = 0.995$, RMSE $(\log_{10}N) \approx 0.021$, MAPE ≈ 3.65%, MdAPE ≈ 2.92%. These quantitative metrics back up the visual parity.

C. *Residual Diagnostics*

Residuals $\Delta\, log_{10}N = \Delta\, log_{10} - \Delta\, log_{10}N_{EXP}$ are centered near zero; histogram and Q–Q plot indicate near-normal dispersion with minimal skew as shown in Fig. 12.

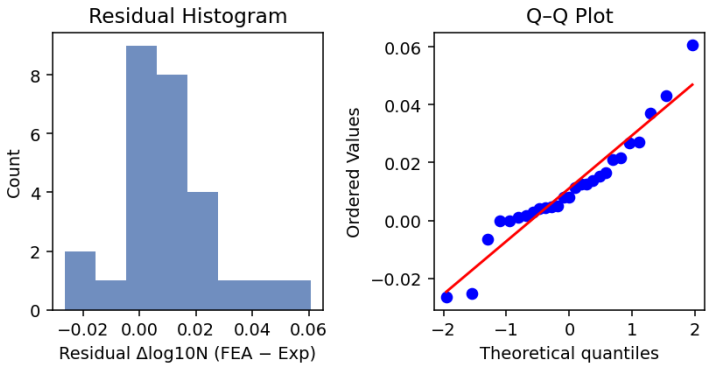

Fig. 12. Residual Histogram and Q–Q Plot for Fatigue Life Prediction Error (FEA vs Experimental)

An agreement (Bland–Altman) view vs. mean log-life confirms no strong bias across life range; 95% limits are narrow, consistent with the small RMSE as shown in Fig. 13.

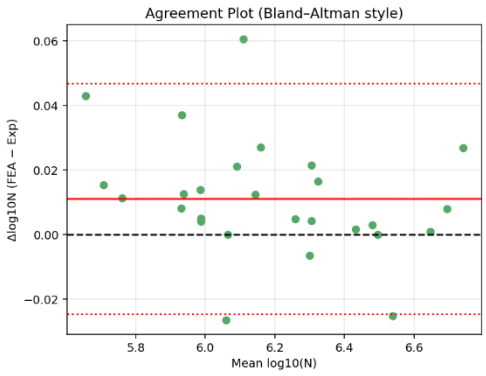

Fig. 13. Bland–Altman Agreement Plot

D. *Frequency–Life Map*

Higher resonant frequencies cluster with a broad life spread, modulated by local stress amplitude is consistent with your combined loading (deadweight & resonant bending) configuration as shown in Fig.14.

International Journal of Engineering Research & Technology (IJERT)
ISSN: 2278-0181
Vol. 15 Issue 03 , March - 2026

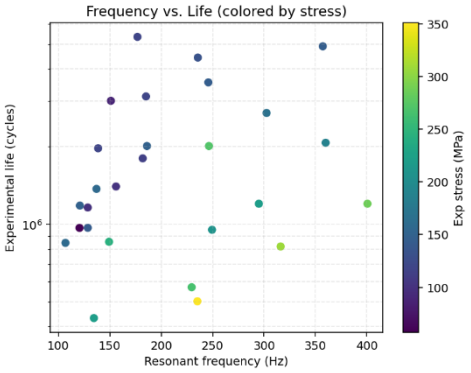

Fig. 14. Resonant Frequency vs Life

E. Effect of Geometrical Parameters

Fig. 15 indicates the variation of fatigue life with applied stress (on a log–log scale) for specimens having one weld (1W), two welds (2W), and three welds (3W). The corresponding trend lines are plotted to compare the influence of weld configuration on fatigue behavior.

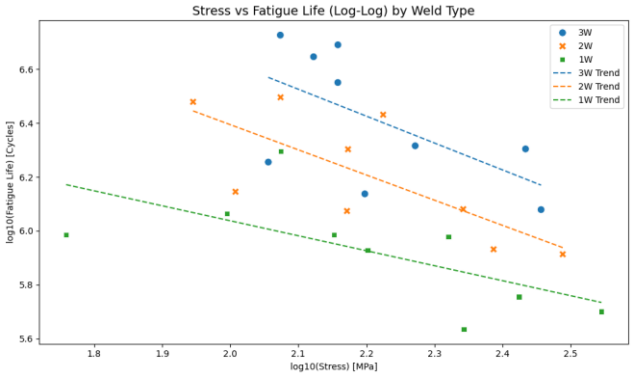

Fig. 15. Stress vs Fatigue Life (Log-log) by Weld Type

From the comparison, it is evident that fatigue life increases with the number of welds, as additional welds help in redistributing stresses and minimizing critical stress concentrations. The trend line separation between 1W, 2W, and 3W specimens remains consistent throughout the stress range, confirming a strong correlation between weld configuration and fatigue performance. For applications subjected to high cyclic loading, the use of multiple welds (preferably 3W) is recommended to enhance fatigue strength and structural reliability. The **best performance** was achieved with the largest diameter (323.8 mm) and thickest wall (1.2 mm), corresponding to the **3W** configuration. The poorest performance occurred for the smallest diameter (141.3 mm) with the thinnest wall (0.511 mm), where stress levels exceeded 300 MPa and fatigue life dropped below one hour. Increasing wall thickness consistently reduced stress concentration and improved fatigue life. Thinner walls (0.511 mm) exhibited higher stresses and premature failure, especially in smaller diameters. For a given thickness, larger diameters showed lower stress levels and longer fatigue life.This can be attributed to reduced curvature-induced bending stress in larger miter bends.

VI. CONCLUSION

The present study investigated the fatigue behaviour of 90° miter bends under resonant vibration using an integrated experimental and numerical approach. An instrumented setup with strain gauges enabled accurate measurement of strain response, which was converted into stress for fatigue life estimation. The results showed strong agreement between experimental observations, Basquin-based predictions, and numerical analysis in log life space, confirming the reliability of the adopted methodology. The study demonstrated that fatigue life is significantly influenced by geometric parameters such as pipe diameter, wall thickness, and number of welds. Specimens with three welds exhibited the highest fatigue life due to improved stress distribution, while single-weld configurations showed early failure due to higher stress concentration. Increasing thickness and diameter enhanced fatigue resistance, whereas higher stress amplitudes reduced fatigue life across all configurations, consistent with classical S–N behaviour. Overall, the findings establish a reliable and practical framework for fatigue life prediction of miter bends under vibration loading, which can be effectively used for design and performance assessment in engineering applications.

International Journal of Engineering Research & Technology (IJERT)
ISSN: 2278-0181
Vol. 15 Issue 03 , March - 2026

VII. FUTURE SCOPE

Future work should generalize the method to realistic service conditions by considering combined pressure, thermal gradients, and multi-axis vibration with variable spectra, while explicitly treating mean-stress and environmental effects (temperature, corrosion/erosion, surface condition). Emphasis should be placed on quantifying fabrication and geometric variability—weld-toe radius, misalignment, out-of-roundness, and residual stresses—and translating their influence on initiation into practical tolerances and inspection intervals. Finally, outcomes ought to be distilled into simple design and maintenance aids (screening charts, checklists) and embedded in reliability-based frameworks that propagate uncertainty to defensible safety factors across the lifecycle.

ACKNOWLEDGEMENT

Grateful acknowledgment is expressed to Dr. Vratraj Joshi and Dr. Dharmin Patel for their valuable guidance, constructive feedback, and encouragement throughout this work.

REFERENCES

[1] Wood, J. “A review of literature for the structural assessment of mitred bends,” International Journal of Pressure Vessels and Piping, 85(5), 275–294, 2008. (Open preprint available via Strathprints).
[2] N. Rathod, D. Patel, A review article on fatigue life estimation of miter bend. J. Mines, Metals Fuels 71(12A), 73–88 (2023). https:// doi. org/ 10. 18311/ jmmf/ 2023/ 43086
[2] Karamanos, S. A. “Mechanical Behavior of Steel Pipe Bends: An Overview,” ASME Journal of Pressure Vessel Technology, 138(4), 041203, 2016.
[3] Karamanos, S. A., Antoniou, K., Keil, B., Card, R. J. “Finite Element Analysis of the Mechanical Behavior of Mitered Steel Pipe Elbows under Bending and Pressure,” Technical paper (public PDF), Northwest Pipe Company, 2020
[4] Li, H., Wood, J., McCormack, R., Hamilton, R. “Numerical simulation of ratcheting and fatigue behaviour of mitred pipe bends under in-plane bending and internal pressure,” International Journal of Pressure Vessels and Piping, accepted manuscript, 2013
[5] Korba, A. G. M. A. Limit and Shakedown Loads for 90-Degree Mitred Pipe Bends under Combined Internal Pressure and In-Plane Bending, M.Sc. Thesis, Cairo University, 2012.
[6] Varelis, G. E., Karamanos, S. A., Gresnigt, A. M. “Pipe elbows under strong cyclic loading,” ASME Journal of Pressure Vessel Technology, 135(1), 011207, 2013. (TU Delft portal summary also available).
[7] Basquin, O. H. “The Exponential Law of Endurance Tests,” Proceedings of the American Society for Testing and Materials (ASTM), 10, 625–630, 1910.
[8] Coffin–Manson (Strain-Life) resources: MIT OpenCourseWare lecture notes “Fatigue: Total Life Approaches—Stress-Life/Strain-Life” (2003) and general LCF primer (Metal Fatigue Life Prediction site)—for background on Coffin–Manson and Morrow relations.
[9] Smith, K. N., Watson, P., Topper, T. H. “A Stress–Strain Function for the Fatigue of Metals,” Journal of Materials, 5(4), 767–778, 1970; and a modern state-of-the-art review of SWT and its modifications (Materials, 15, 3481, 2022) for extended context.
[10] Neuber, H. Theory of Notch Stresses: Principles for Exact Calculation of Strength with Reference to Structural Form and Material, USAEC Office of Technical Information, 2nd ed., 1961. (Catalog and open-access pointers). [fde.uwaterloo.ca], [becht.com], [researchgate.net]
[11] Vibration-induced fatigue guidance (EI AVIFF & case practice): ASME PVP2024 paper “Case Histories of the Resolution of Piping Vibration Failures in the Oil and Gas Industry” referencing Energy Institute (EI) AVIFF methodology; and Becht training deck “Assessment and Resolution of Piping Vibration” summarizing stepwise protocols.
[12] ASME B31.3 Process Piping—context and guidance documents (LANL/LBNL Process Piping Guide Rev. 2, 2009) and practice discussions on miter bend clauses and analysis considerations.
[13] K. Takahashi, S. Tsunoi, T. Hara, T. Ueno, A. Mikami, H. Takada, and M. Shiratori, Experimental study of low-cycle fatigue of pipe elbows with local wall thinning and life estimation using finite element analysis. Int. J. Press. Vessels Piping 87, 211–219 (2010). https://doi.org/10.1016/j.ijpvp.2010.03.022
[14] M. Sarrate, A. Huerta, and J. C. Cajas, “Advances in hexahedral mesh generation for finite element analysis,” Arch. Comput. Methods Eng., vol. 29, pp. 2481–2503, 2022
[15] M. Cesnik and J. Slavic, “Vibrational Fatigue and Structural Dynamics for Harmonic and Random Loads,” Strojniski vestnik – Journal of Mechanical Engineering, vol. 60, no. 5, pp. 339–348, 2014. DOI: 10.5545/sv-jme.2014.1831
[16] N. Rathod, D. Patel, Development of machine learning regression models to assess Von Mises stresses of miter bend. J. Inst. Eng. India Ser. C, Volume 106, 749-764 (2025). https://doi.org/10.1007/s40032-025-01181-0
[17] M. Govindasamy, G. Kamalakannan, and G.K. Meenashisundaram, “Vibration-Based Structural Health Monitoring of Laminated Composite Beams Using Finite Element Modal and Harmonic Analysis,” J. Compos. Sci., vol. 10, no. 2, pp. 79, 2026.
[18] F. Kun, H.A. Carmona, J.S. Andrade Jr., and H.J. Herrmann, “Universality behind Basquin’s law of fatigue,” Phys. Rev. Lett., vol. 100, 2008.